JOURNAL OF AIRCRAFT
Vol. 48, No. 2, March–April 2011

Transient Poststall Aerodynamic Modeling for Extreme Maneuvers in Micro Air Vehicles

Gregory W. Reich*
U.S. Air Force Research Laboratory, Wright-Patterson Air Force Base, Ohio 45433
Franklin E. Eastep† and Aaron Altman‡
University of Dayton, Dayton, Ohio 45469
and
Roberto Albertani§
University of Florida, Shalimar, Florida 32579

DOI: 10.2514/1.C000278

This paper addresses the modeling of transient aerodynamic behavior at angles of attack near and well above stall. These angles of attack are seen in extreme maneuvers of micro air vehicles (in this case, perching), where unsteadiness results from variations in angle of attack, planform changes, or other physical reconfiguration. To study the problem, a mechanized wing concept for a perching micro air vehicle was developed to produce wing rotation to high angles of attack. Wind-tunnel tests were conducted to measure static and dynamic vehicle performance and flight-control parameters. Test results were compared with a first-order lag model, used to describe the delay in response due to wing rotation, coupled with a simple aerodynamic analysis. Results demonstrate that the first-order lag is effective in capturing unsteady effects due to wing rotation. In situations where three-dimensionality of the flow dominates, a more complex model may be required.

I. Introduction

INTEREST in the design and development of birdlike micro air vehicles (MAVs) has emerged in recent years. While the definition of what constitutes a MAV varies widely, this class of vehicles can be generally characterized by low flight speed, small size, and a low Reynolds number. One mission scenario for a MAV is to travel covertly into hostile territory to collect and transmit data. Creating a MAV that acts and looks similar to a bird allows the vehicle to hide in plain sight, meaning that the vehicle would not stand out or look out of place in the environment in which it was operating.

Research in the area of birdlike MAV development has focused strongly on the aerodynamics of flapping and on the kinematic motion of the wings, as well as guidance, flight dynamics, and vehicle control. Recently, the U.S. Air Force Research Laboratory has initiated research into a perching MAV, one where the vehicle uses a trajectory similar to a bird landing on a wire or branch. Issues related to unsteady aerodynamics, flight control, vehicle design, mechanization, power requirements, etc., must all be addressed in order to achieve maneuvers of this type. Ultimately, the goal of the project is to create biomimetic bird-sized MAV that can perch. In this paper, the aerodynamic behavior of such a vehicle is investigated and a numerical method for describing the behavior is developed.

Perching can be defined as landing with approximately zero vertical and horizontal velocity on a specific point. Birds use several specific maneuvers to complete this type of landing. Often, birds flap their wings at a high frequency for a short period of time in order to create additional lift as they land with negligible flight speed. Birds also rotate their bodies and wings to significantly high angles of attack, up to 90 deg, in order to increase the wing surface area in the direction of the flight path, increasing drag to reduce horizontal flight speed. Additionally, birds often assume an ascending path toward the end of their trajectory. A bird will fly below its landing target and pull upward at the end of the flight path to exchange kinetic for potential energy. In this project, we choose not to use flapping but rather focus on landings similar to raptors [1] that demonstrate the latter two features.

Perching as a topic has not received a great deal of attention in the research community. Wickenheiser and Garcia [2] have investigated perching maneuvers for a morphing unmanned air vehicle (UAV) designed to explore the Martian atmosphere. They address longitudinal flight dynamics, as well as trajectory optimization and aerodynamic modeling, incorporating a time delay aerodynamic model to account for fluid transients in the region of stall [3]. Recently, Cory and Tedrake [4], Hoburg and Tedrake [5], and Moore and Tedrake [6], at the Massachusetts Institute of Technology, have investigated the use of exclusively linear models to control fixed-wing maneuvers for perching on a wire. The U.S. Air Force Academy has developed a concept for perching on vertical surfaces using an adhesive pad attached to the nose of the vehicle [7]. Finally, a mechatronics group at Stanford University has demonstrated a perching maneuver using a foam UAV that incorporates a clinging mechanism for vertical surfaces [8].

In the realm of unsteady aerodynamics, the least computationally expensive method employed to predict the aerodynamics associated with a bird-perching maneuver is the Wagner function. One of the Wagner function's most important underlying assumptions is linear aerodynamics resulting from the application of two-dimensional (2-D) potential flow theory to the nonuniform motion of airfoils, which is a common thread throughout many of the methods described here. Wagner's function is an indicial admittance function and describes the change in circulation/lift resulting from the impulsive start of an airfoil at a small fixed angle of attack taken to some steady final velocity. This small angle assumption is also inherent in many of the methods described and provides a significant impediment to the application of these methods to the perching problem without substantial validation.

Presented as Papers 2009-0063 at the 47th AIAA Aerospace Sciences Meeting, Orlando, FL, 5–8 January 2009; received 26 January 2010; revision received 7 May 2010; accepted for publication 1 July 2010.

*Senior Research Engineer, Air Vehicles Directorate, 2210 8th Street, Room 219. Associate Fellow AIAA.
†NRC Faculty Fellow, Mechanical and Aerospace Engineering, 300 College Park. Associate Fellow AIAA.
‡Associate Professor, Mechanical and Aerospace Engineering, 300 College Park. Associate Fellow AIAA.
§Research Assistant Professor, Research and Engineering Education Facility, 1350 North Poquito Road. Member AIAA.

Complementary to Wagner's function is Theodorsen's function, which describes the lift due to circulation for an airfoil oscillating sinusoidally while moving at a steady velocity. Theodorsen's function also depends on a small angle assumption, and it is often given as the sum of two parts: a classical noncirculatory contribution and a circulatory contribution. This manner of separating relative contributions to the lift force is quite versatile for enveloping the effects of additional circulation and is analogous to a number of more advanced methods that will shortly be discussed. Wagner's and Theodorsen's functions, as well as an additional function called Kussner's function that describes the lift response to an impulsively applied vertical gust, are well detailed in a 1938 NACA report by Garrick [9].

In 1981, McCroskey [10] documented a resumé of unsteady aerodynamic techniques as applied to dynamic stall and helicopter rotor aerodynamics. While many of the methods and discussions from the paper are not pertinent, as the flow environment for helicopter flight is quite different than for perching, a few of his observations are valid. In particular, McCroskey observed that sweep tends to delay the onset of dynamic stall and reduces the rate of change of C_L and C_m as stall begins. This observation is particularly relevant when three-dimensional (3-D) effects due to planform shape change in perching are considered. Sweep also reduces the magnitude of the hysteresis loops somewhat.

McCroskey [10] also observed that in the light stall regime, the leading-edge (LE) geometry of an airfoil is a principal factor in determining boundary-layer (BL) separation characteristics. He notes that airfoils with moderately sharp LEs tend to develop severe adverse pressure gradients in the first few percent of chord, leading to abrupt BL separation that spreads rapidly downstream (usually LE stall). This contrasts with trailing-edge (TE) stall, which is more common on airfoils with relatively blunt noses or large amounts of LE camber. In this case, the BL separation progresses forward from the TE, the onset of stall tends to occur more gradually, and unsteady effects tend to suppress the separation more than on LE stall airfoils.

For a good survey of methods for analysis of generic unsteady airfoil flows, Cebeci et al. [11] provides a number of techniques. The applicability of most of these methods to the perching problem is somewhat limited by their underlying assumptions; however, the text does provide a sufficiently broad survey of methods to serve as an excellent foundation for understanding some of the methods more appropriate to perching.

Additionally, there have been numerous implementations of unsteady vortex-lattice methods and quasi-finite wake implementations of potential flow methods. All of these methods suffer from the same limiting fundamental potential flow assumptions. In an attempt to circumvent the drawbacks of the inviscid assumption, Gulcat [12] provides an unsteady viscous–inviscid interaction model where the surface velocity distribution is used as the edge velocity of the unsteady BL to predict the viscous effects in flapping wings. This method was found to work well up to the effective angle of attack of dynamic stall.

As a rule, the more completely and accurately the potential flow methods model the wake, the more computationally expensive they become. If they include vortex shedding, they require some form of empirical tuning to determine the correct frequency/convection times. Of course, computational fluid dynamics (CFD) methods represent the upper end of fidelity for this type of model. Because of the expense of computation, they are not suitable for design, and therefore are not considered here. All of the aforementioned methods, with the exception of the Wagner function, can be applied more to quasi-steady cruise-flight-type flapping and not necessarily to perching.

A number of state-space-type models have also been created. These models are much better suited to real-time flight dynamic and control implementation due to the nature of their reduced order. Of note, a non-physics-based model of dynamic stall similar in form to the ONERA model mentioned by McCroskey [10] was documented by Magill et al. [13]. Their model takes into consideration three mechanisms involved in the flow dynamics:

1) The model solution was required to relax to the steady pressure solution at a steady pitch angle.

2) A term resembling circulation addition is added to the flow as the wing pitches.

3) Two different mechanisms were provided for the relaxation from transient to steady pressure depending on the angle of attack.

The separation dynamics consisted of a second-order relaxation to the steady separation condition. The three aforementioned mechanisms are manifested in the equations by a convective relaxation term, circulation addition term, and the dynamic stall vortex shedding influence term. Ultimately, the model was tested and compared well at reduced frequencies of 0.05 and 0.1 for the pitchup case but not the pitchdown case, which has proven more problematic from a modeling standpoint [14].

Ahuja et al. [15] used balanced proper orthogonal decomposition to develop observers to reconstruct the flow state; however, this requires knowledge of a single surface pressure measurement. This approach was later modified slightly [16] and compared with more direct-numerical-simulation computational models and experiments at a Reynolds number of 300 and a reduced frequency of 0.5. The results in comparing 2-D and 3-D results were mixed, placing caveats on the application of the model. They did show the ability to construct a three-state nonlinear ordinary-differential-equation model that agrees well with the transient and steady-state lift on an impulsively started plate at fixed angle (across a range of 0 to 90 deg alpha). Although this model requires tuning using parameters extracted from experiments, it shows that because the behavior is deterministic, it is possible to construct a relatively low-order model, which agrees very well with the data.

This project investigates the possibility of a MAV that can perch without using flapping. In the short term, the team has a number of aims: 1) to investigate the degrees of freedom required to mechanize the wings for landing and the power required to perform this motion, 2) to understand the aerodynamic behavior of transient wing motions at high angles of attack, and 3) to develop a simple numerical model that can be used to predict the performance of different designs. To this end, a wind-tunnel model of a notional MAV was developed to investigate mechanization issues and power requirements as well as aerodynamic response to transient wing motions [17,18]. A second set of wind-tunnel tests [19,20] have been completed to get a more accurate understanding of both the static and transient loads in this low-speed high-angle-of-attack regime. In this paper, the authors discuss these results, investigate several numerical models, and compare their load predictions to the wind-tunnel results.

II. Model Description

Most of the material in this section is taken from the previous papers by Lukens et al. [17,18] and Reich et al. [19,20] and is presented here as a review. Design requirements for the conceptual vehicle were developed based on flight maneuvers of birds and wing/body kinematics [21]. Based on this understanding, two degrees of freedom were chosen for each wing. These degrees of freedom correspond to wing twist at the shoulder and an independent wing twist at the wrist. Once this mechanization concept was determined, pigeon geometry and weight was used for load approximation and structural sizing.

The model consists of a fuselage and attached wings, as depicted in Fig. 1. Note that the entire span is broken into four sections, symmetrical about the fuselage. The wing actuators, completely contained within the fuselage, allow each section of the wings to rotate up to a wing incidence angle of 90 deg. The model has a wingspan of 61 cm and a chord of 11 cm. The thickness ratio of the wings in this model is 9%, which allows for room within the wings for structural members [22]. For the first prototype, a NACA 0009 airfoil is used. The shape of the fuselage was chosen to be a symmetric airfoil with a high thickness-to-chord ratio: approximately a NACA 0035. The model structure is constructed of balsa with carbon-fiber spars and a Mylar skin.

To mimic wing motion during perching, the wings are capable of rotating to a wing incidence of 90 deg. Each wing consists of two joints and two wing sections: a proximal wing section (closest to the fuselage) and a distal wing section (farthest from the fuselage). The

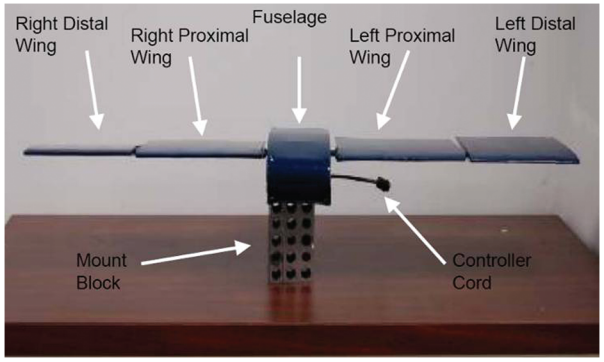

Fig. 1 Model configuration: head-on view.

shoulder joint is located at the root and the wrist joint is located nearly halfway along the span, 14.9 cm from the root. The two proximal wings are attached to a single spar driven by one actuator so that they maintain the same wing incidence. The distal wing sections are each driven by their own independent actuator. The wing spars are sized such that the maximum safe loads on the model are attained when all wing sections are oriented at 90° at 5 m/s, 45° at 7.5 m/s, and 10° at 10 m/s.

III. Test Setup

Testing took place at the University of Florida Research and Engineering Education Facility MAV Aerodynamic Characterization Facility in late July of 2008. The open-section wind tunnel is a new facility specifically designed for low-speed testing of MAVs. The objective of these tests was to acquire accurate data in the wind tunnel at very low speeds in a low-turbulence controlled flow. The test setup, some of which is shown in Fig. 2, consisted of the model, sting balance, high-speed cameras, and a data acquisition (DAQ) system that recorded 10 channels of data: six aerodynamic forces and moments, and two voltages and two currents related to the power required to drive the actuators. A stereoscopic image system with two high-speed cameras was used to produce 3-D estimates of the model position. This information created measurements of the wing angles via appropriate visual image tracking software and postprocessing. Tunnel operating parameters such as velocity, temperature, and pressure were also recorded for later use.

The DAQ system actually recorded data in three separate groups. The force balance, a high-sensitivity six-component transducer from Allied Aerospace (model MC-.03-.300), measured aerodynamic forces and moments that were converted to forces and moments at the model center of gravity. These data, along with the tunnel operating and atmospheric conditions, was sampled at a rate of 77 Hz by the main DAQ computer using a National Instruments PXI module. The second group, consisting of the actuator voltage and current inputs, was sampled at a rate of 1000 Hz by the main DAQ using a National Instruments SCXI module. Finally, the high-speed cameras (Vision Research Phantom V7.1) recorded images on a separate computer at a variable rate between 10 and 200 Hz, depending on the particular test run. Because all of these systems were separate, synchronization was required in postprocessing to align the events with the data in time. Control of the wing motion was done through yet another computer, using a graphical user interface supplied by Parallax, Inc. [23] that communicated with the actuator control board via Universal Serial Bus (model 28823). Other postprocessing done on the aerodynamic data included corrections for streamline and downwash related to the wind-tunnel BL. These corrections applied to the angle of attack, drag coefficient, and pitching moment coefficient.

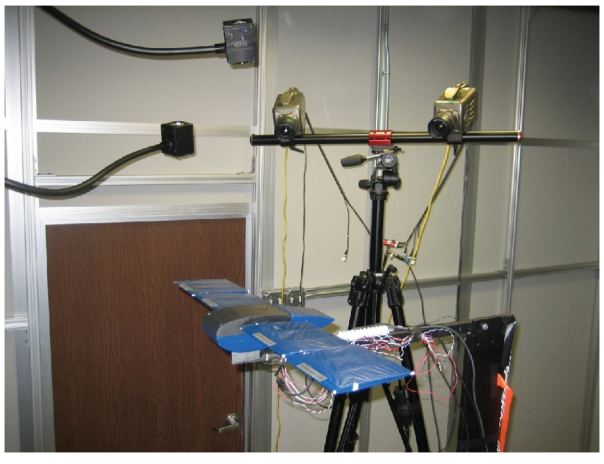

Fig. 2 Test setup showing model, sting, and cameras.

IV. Test Results

Experiments were carried out in two phases. In the first phase, averaged steady-state measurements were taken at a variety of wing incidence angle combinations in order to build a quasi-steady matrix of control derivatives. These were done at flight speeds between 1 and 10 m/s. In the second phase, time histories of loads and power required were recorded for transient wing motion at different rotation speeds over a similar range of incidence angles and flight speeds. Since the focus of this paper is on aerodynamic modeling, and the fact that the power data have been discussed in previous papers [17–19], the power measurements will not be discussed further.

A. Static Tests

Static tests were completed at 1, 5, 7.5, and 10 m/s. At 1 m/s, the forces generated were within the noise of the sensor, and so these results will not be discussed. At each test point, 20 ensembles of 500 samples were averaged together to get the results shown. The static test results are all presented in the same manner in Figs. 3–5. The top plot shows the wing angles at each point in the test sequence. The middle plot shows the normal and axial force coefficients (lift and drag), along with the 95% confidence intervals at each point. The bottom plot shows the pitching moment coefficient about the wing aerodynamic center, along with the 95% confidence interval.

At 5, 7.5, and 10 m/s, shown in Figs. 3–5, respectively, the data reveal nothing of a surprise. The loads increase as the tunnel velocity increases, and the lift and drag behave as they would be expected to behave, both below and above stall. Below stall (which in this case is estimated to be around 12 deg), the lift and drag increase with angle of attack, while the pitching moment is nearly constant (note that the

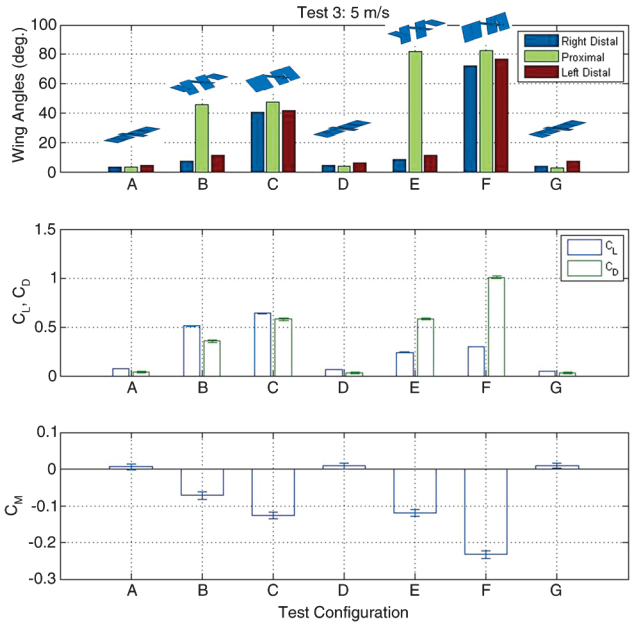

Fig. 3 Static test results for 5 m/s.

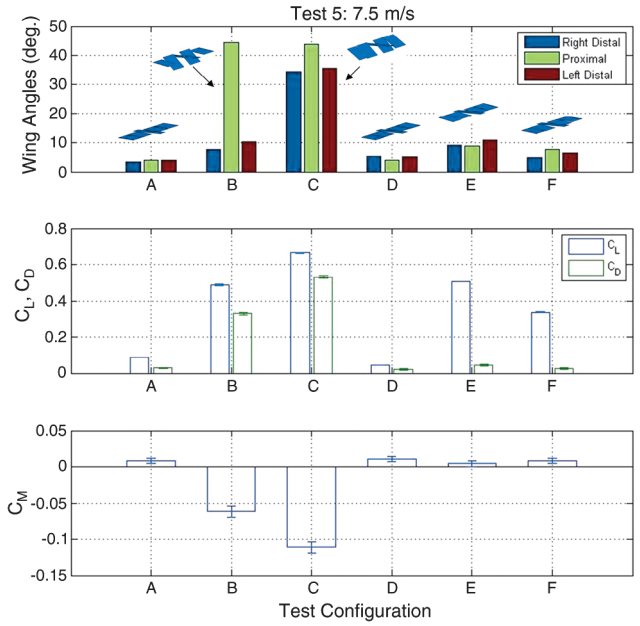

Fig. 4 Static test results for 7.5 m/s.

vertical axis scale for the pitching moment coefficient in Fig. 5 is very small and the overall change in moment is almost nil). Above stall, the drag increases significantly, the pitching moment decreases significantly, and the lift increases until about 45 deg and then reduces again. These results match nicely with other wind-tunnel results [24,25] of similar airfoils and finite wings at steady angles of attack above stall.

Better evidence of the angle-of-attack-dependent behavior can be seen in Fig. 6, which demonstrates static results as the wing incidence angles are increased as a group from zero up to almost 90 deg. A better view of this response with respect to angle of attack is shown in Fig. 7, in which the force and moment coefficients are plotted versus the average angle of attack of the wing sections. Data are taken at a number of low angles up to about 16 deg but then jump up to 25 deg, so the drop in lift at stall is not clearly captured. However, the trends in all three coefficients are as expected and match up with other published sources of similar data [24,25].

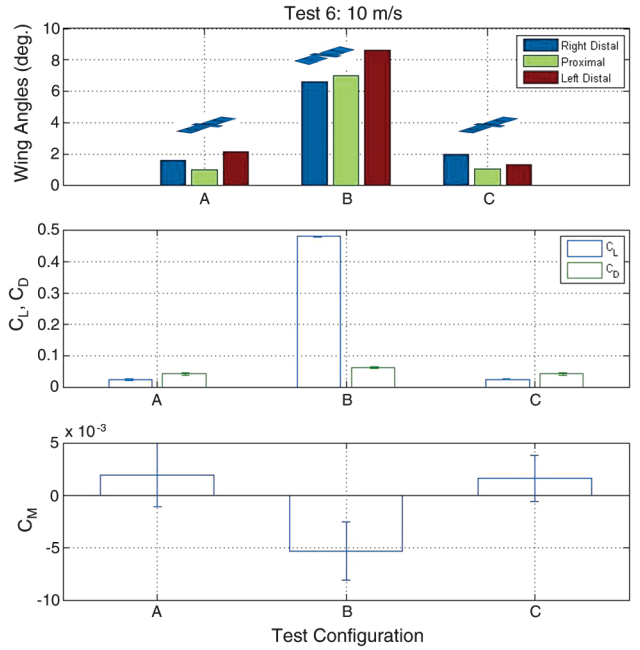

Fig. 5 Static test results for 10 m/s.

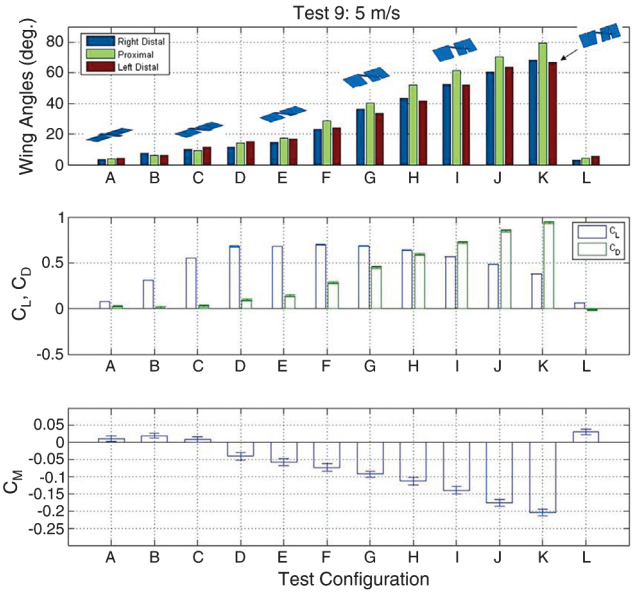

Fig. 6 Static test results for synchronized sweeping motion at 5 m/s.

B. Dynamic Tests

Of more interest to the ultimate goals of the project are dynamic tests, where time histories of aerodynamic data were recorded during single runs with wing motions at different rates. Data in this section will be presented in several different ways. For example, Fig. 8 shows the wing angles amd force and moment coefficients for a run at 10 m/s. For this particular run, the wings are rotated together from 0 to 10° and back down. The data are very benign as all of the wing angles are well below stall, so that basically no variation in drag or pitching moment are seen. What is interesting is that the wing angles exhibit significant vibration in the wings at this flight speed. It is possible that there was a limited aeroelastic behavior, such as limit cycle oscillation due to the freeplay, but this was not investigated to any extent.

Data at 5 and 7.5 m/s were taken for a number of wing profile sweeps and a range of wing rotation rates. Rather than presenting a large amount of data with different combinations of proximal and distal wing angles, rotation rates, and flight speeds, one simple set of runs are presented in Figs. 9–11. For this set of runs at 5 m/s, all of the wing angles are commanded to move together in a single motion from 0 up to 85° and back down to 0. The three rates, labeled fast, medium, and slow, are approximately 160, 50, and 8°/s, corresponding to reduced frequencies k [as defined by Eq. (1)] of 0.03,

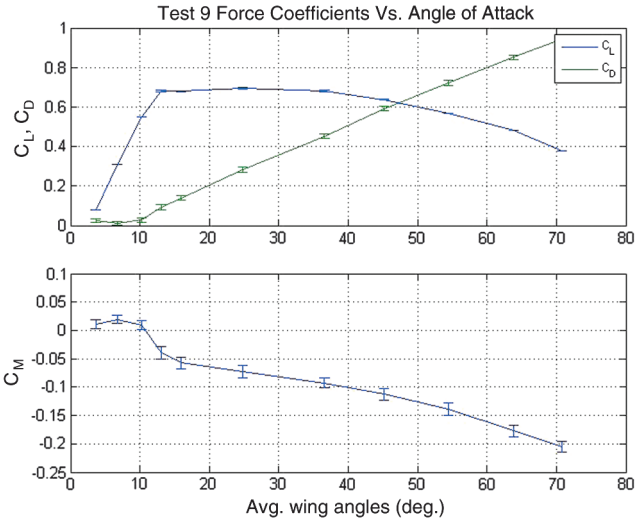

Fig. 7 Static test results for synchronized sweeping motion at 5 m/s plotted versus the average wing incidence angle.

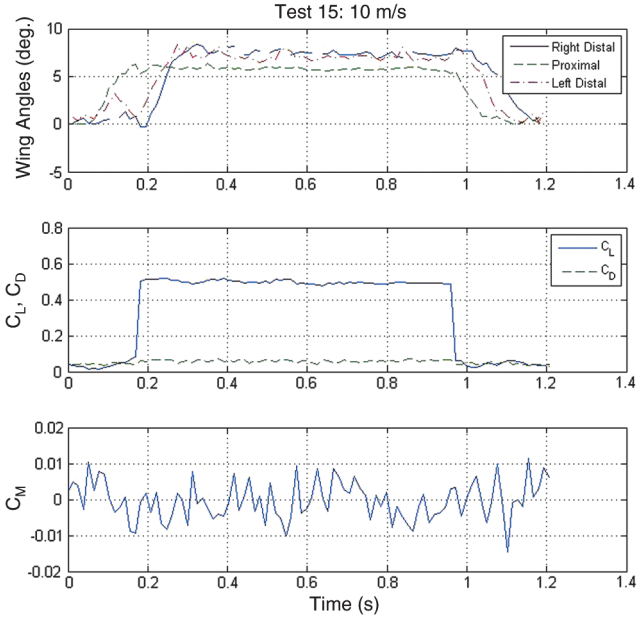

Fig. 8 Dynamic test results at 10 m/s.

0.01, and 0.002. (Note that these numbers do not match those quoted in the conference papers [19,20], as a different definition of reduced frequency was used for earlier calculations.) While these numbers are small as compared with many flapping fliers [26], the fastest one is in the range where unsteady effects due to circulation become important:

$$k = c\dot{\theta}/2U_\infty \tag{1}$$

A feature to note immediately is that the distal wings never reach the commanded wing angles. For the fast rotation rate, it is possible that the distal wings are never given the chance to set at the same angle as the proximal. For the slower profiles, however, there is sufficient time for that to happen, so it is most likely due to misalignment in the mechanism as the testing progressed. The mechanism itself was very fragile, not something that would be built into an actual operational vehicle, and demonstrates the importance of precision manufacturing and design for a robust, accurate mechanism to drive wing rotation and other degrees of freedom.

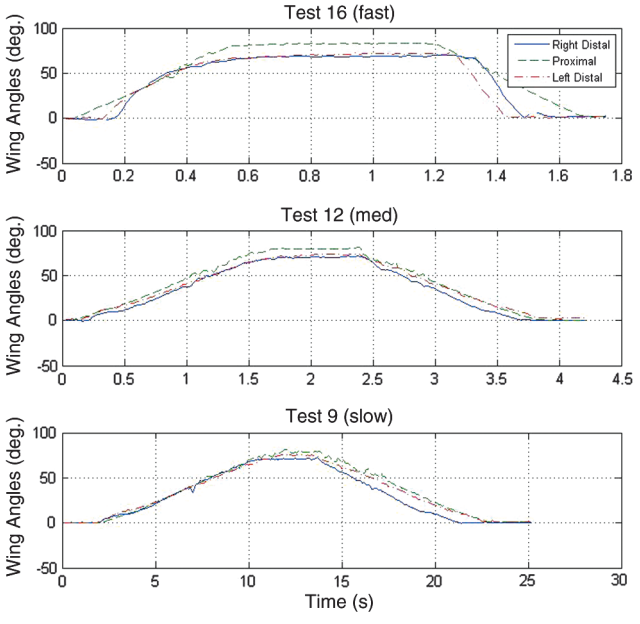

Fig. 9 Wing angle profiles for three synchronized runs at 5 m/s.

In Fig. 11, the difference between steady flow and dynamic stall effects can clearly be seen. In this and the following figure, the time axis has been normalized so that all three results can be plotted together for comparison. Because the actual wing profiles were triggered manually, the starting and stopping times cannot be compared, but the relative magnitude and shape of the lift coefficient curve can be evaluated for the different rotation rates. The fast response in blue shows a large peak in lift force above the expected maximum C_L, even for poststall behavior. At the back end of this profile, there is not a corresponding peak as the wing angles return through 45° or stall, as the flow has not been able to reattach to the wings.

In contrast to this response is the behavior at smaller rotation rates. At the medium rotation rate, there is a small increase in lift for positive rotation and a similar decrease for negative rotation, which is generally the expected trend for a quasi-steady flow. At the small rotation rate, this is even more pronounced. The difference in lift force between positive and negative rotations is very small, and it is even possible to see a little of the stall dip on the back side around $\bar{t} = 0.85$.

V. Modeling

The ultimate goal of the project is to create a perching MAV design. To advance through the design process, an analysis tool is required that can quickly and accurately predict the transient poststall/postseparation behavior of the vehicle during perching maneuvers. Because it is to be used for vehicle and flight-control system design, speed is more important than accuracy, which means that CFD methods cannot be considered practical.

A few early attempts have been made to model the perching maneuver. Several have assumed flat plate aerodynamic behavior either throughout the range of angle of attack [4] or only in the poststall regime [3]. In a previous paper [18], a tool is described that incorporates a simple steady aerodynamic model using experimental data for quasi-steady poststall forces. That model jumped directly between attached and stalled flow based on the maximum lift coefficient on each wing section. Other authors [3] have used the first-order time delay suggested by Goman and Khrabrov [27] to model the effects of separation during wing rotation; viz.,

$$\tau_1 \dot{p} = p_0(\alpha - \tau_2\dot{\alpha}) - p \tag{2}$$

where p is an aerodynamic state, p_0 is a mixing function between attached and separated flow, and τ_1 and τ_2 are empirical time scales related to the transient flow response to disturbances and delays in flow separation and reattachment, respectively. We will apply this model to the current results in order to develop a model suitable for rapidly investigating different conceptual designs in a short period of time.

The use of this first-order time delay has been demonstrated to work for delta wings and for poststall aerodynamic models [27]. Here, the manner in which this model might be incorporated into different aerodynamic models to capture the effects of separation is examined. To start, we will focus solely on the total lift on the model, with the understanding that drag and pitching moments can be handled similarly. Following Wickenheiser and Garcia [3], the aerodynamic model is divided into separated and attached flows, where

$$C_{L,\text{sep}} = 1.1\sin(2\alpha) \tag{3}$$

is a simple curve fit to a complete steady lift curve for the given airfoil section [24]. A number of different attached lift coefficients are considered, from the most simple 2-D lift curve slope to a finite wing-corrected unsteady lift that incorporates apparent mass and circulation:

$$C_{L,\text{att},S} = a_0\alpha \tag{4}$$

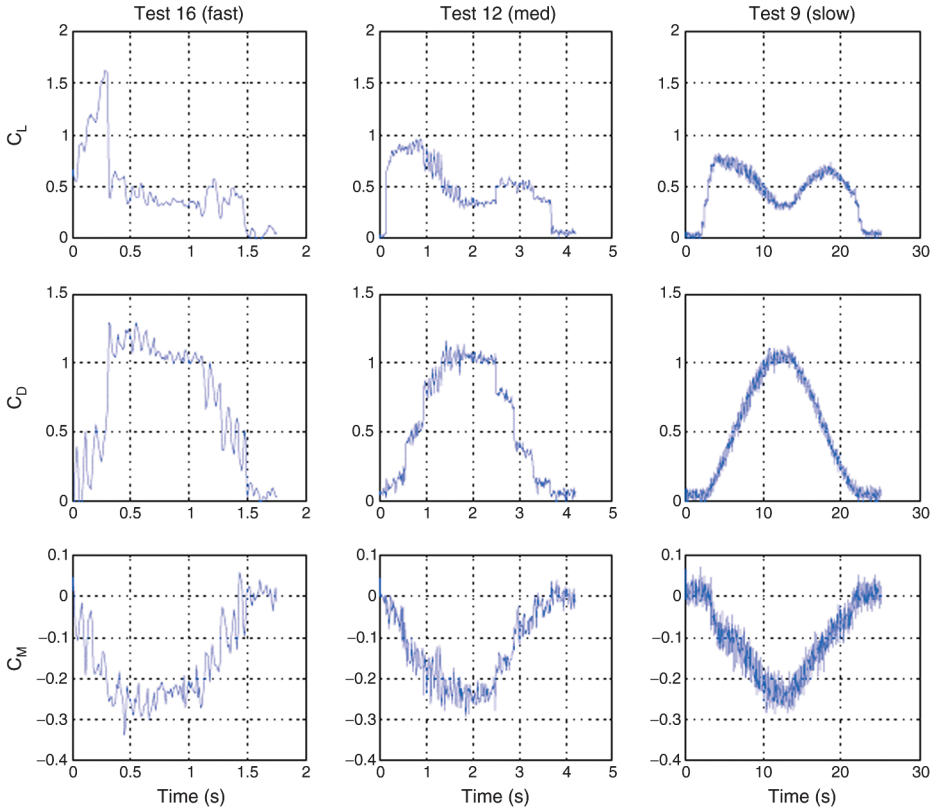

Fig. 10 Force and moment coefficients for three synchronized runs at 5 m/s.

$$C_{L,\text{att,FW}} = \bar{a}\alpha = \frac{a_0\alpha}{1 + a_0/\pi e\text{AR}} \tag{5}$$

$$C_{L,\text{att,QS}} = a_0\left\{\frac{b}{2U}\dot{\alpha} + \alpha + \frac{b}{U}\left(\frac{1}{2} - a\right)\dot{\alpha}\right\} \tag{6}$$

$$C_{L,\text{att,QSFW}} = \bar{a}\left\{\frac{b}{2U}\dot{\alpha} + \alpha + \frac{b}{U}\left(\frac{1}{2} - a\right)\dot{\alpha}\right\} \tag{7}$$

where $a_0 = 2\pi$ is the 2-D lift curve slope, $\bar{a}$ is the 3-D lift curve slope, e is Oswald's efficiency factor, AR is the aspect ratio, U is the flow velocity, b is the semichord, a is the offset between pitch location and midchord, and the subscripts S, FW, QS, and QSFW refer to steady, steady finite wing, quasi steady, and quasi-steady finite wing models, respectively. Note that the latter two lift coefficient forms (QS and QSFW) represent unsteady flow in and of themselves with the incorporation of rotation rate, but they say nothing about the delay inherent in the system and are thus considered quasi steady. Note also that the delay parameters τ_1 and τ_2 from Eq. (2) both scale with the characteristic time scale b/U.

To combine the two regions of flow, the mixing function p_0 is defined as the following sigmoid function [3]:

$$p_0(\alpha) = \begin{cases} 1, & |\alpha| < 4^\circ \\ -.3326\tan^{-1}\left(\frac{180}{\pi}|\alpha| - 16\right) + 0.5, & 4^\circ < |\alpha| < 37^\circ \\ 0, & |\alpha| > 37^\circ \end{cases} \tag{8}$$

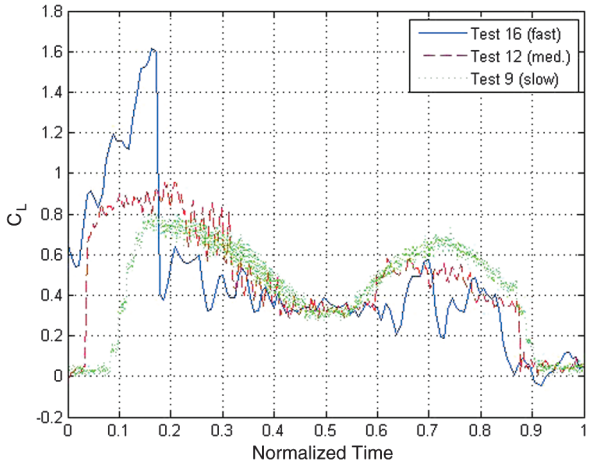

Fig. 11 Comparison of lift coefficients for three wing rotation rates at 5 m/s.

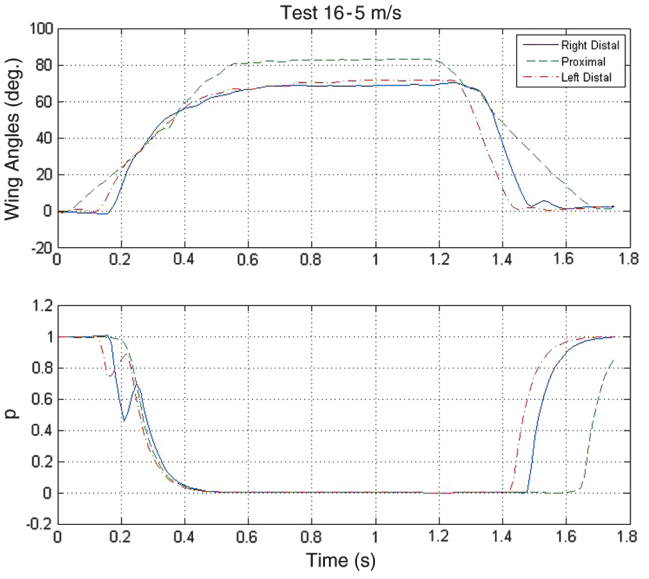

Fig. 12 Wing section angles (splined) and aerodynamic state parameter p for test 16.

This function provides a smooth transition from a value of one at small angles of attack (no separation) to a value of zero (fully separated) at large angles of attack. Combining the effect of Eqs. (2–8), the total lift coefficient for each wing section at a given angle of attack can then be determined as

$$C_L(\alpha, \dot{\alpha}) = C_{L,\text{att}}(\alpha, \dot{\alpha}) \cdot p(\alpha, \dot{\alpha}) + C_{L,\text{sep}}(\alpha) \cdot [1 - p(\alpha, \dot{\alpha})] \quad (9)$$

As an example, results from test 16, seen as the fast results in Figs. 9–11, are used to compare experimental and numerical results. First, splines of the time histories of wing section incidence angles are created in order to more easily compute $\dot{\alpha}$. Note that these splines accurately recreate the measured wing angles, and they produce smoother $\dot{\alpha}$ curves than a finite difference scheme would. Next, the time delay equation (2) is solved to determine a time history of the aerodynamic state p for each wing section. These two pieces are then combined in Eqs. (3–7) and (9) to compute the complete lift coefficient for each wing section, which are then summed to find the total lift on the vehicle.

One other model is used to predict the wind-tunnel loads based on the wing angle profiles. This is a vortex-lattice code embedded into a vehicle simulation tool [28] developed for simulation of morphing vehicles. In the simulation, the full vehicle is modeled, and the splined wing angle profiles are used to directly move the wing sections. Aerodynamic loads are computed at each time step based on the current geometry. The vortex-lattice code is an in-house code that allows for unsteadiness in boundary conditions but not in wake behavior. At each time step, the wake is assumed to be a flat vortex sheet propagating back from the TE of each wing panel section. At each time step, for each wing section, both attached (vortex lattice) and separated lift coefficients are computed, and these are combined based on the time delay mixing parameter as in Eq. (9).

A relevant aspect to mention here is that the pitching moment is a critical parameter for this type of maneuver. The pitching moment, as seen in Fig. 10, is highly negative (i.e., nose down) at large angles of attack, exactly when the vehicle is pitching nose up to get to those large angles. Alleviation and control of this behavior is vital. However, for the discussion that follows, we will focus solely on the lift force, with the optimistic assumption that drag and moment can be handled in a similar fashion.

VI. Results and Discussion

Results from all of these models are shown in Figs. 12 and 13. Figure 12 shows the wing section incidence angle time histories on top and the aerodynamic state parameter p on the bottom. Figure 13 contains both the wind-tunnel experimental result and five different numerical results corresponding to Eqs. (4–7) and the vortex-lattice-based simulation, labeled VL in the figures.

In Fig. 12, comparison of the wing angles with the aerodynamic state parameter p gives a clear indication of the time delay in the system. In the figure, for instance, at 0.2 s, the proximal wing angle is at an approximately 25 deg angle of attack, which typically would be considered a separated flow condition. However, p for this wing section is nearly one, meaning that the lift force contribution is almost entirely from attached flow. The distal wing sections show similar behavior, although with a hump in the mixing parameter. It is unclear to the authors exactly why this occurs, but one hypothesis is that this is an artifact of the spline used to curve fit the experimental wing angle-of-attack data. The effect of time delay can also be seen at the end of the test run, where the wing section angles have all returned to small angles of attack, nominally attached flow conditions, but the corresponding state parameters indicate that lift force contributions are based on separated flow.

In comparing the different models used to compute lift force, only small differences can be seen in Fig. 13. Note that all four models from Eqs. (4–7), even the finite wing models, are truly 2-D and do not account for 3-D flow effects beyond a simple steady-state correction to the lift curve slope. Additionally, all four models fail to accurately capture the behavior during the downward rotation back through stall, which is consistent with other studies of similar phenomenon

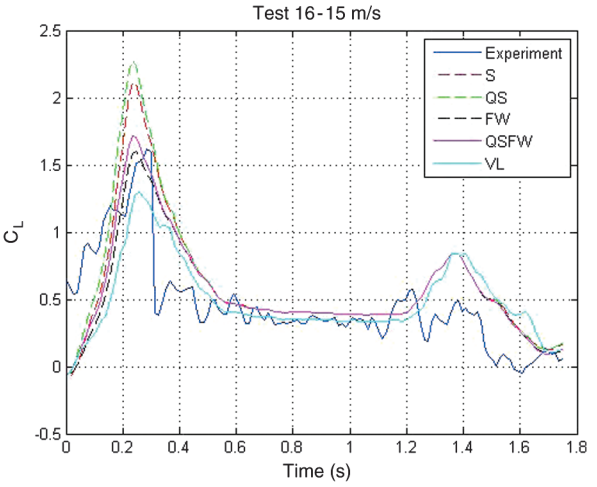

Fig. 13 Comparison of lift coefficient computations for test 16.

[14]. The vortex-lattice model incorporates both 3-D effects (finite wing and influence between wing sections) as well as unsteadiness (moving boundary condition). All five versions incorporate the same poststall model, which is a 2-D lift curve slope based on experimental data [24]. In every case, a large lift coefficient is predicted as the wing sections come back down through stall. This is not the case for the experimental data, and suggests that more work is needed in order to capture the flow behavior in this regime. Note also that all five models use the same time delay, and all capture the location of the lift peak in time with reasonable accuracy. For the test results shown in this section, the values for τ_1 and τ_2 are $4.55b/U$ and $6.82b/U$, respectively.

Additional data sets have been analyzed to validate the models; however, only one other data set is presented here. This test, the results of which are shown in Figs. 14 and 15, took place at 7.5 m/s, with wing angles up to 45 deg. In contrast to previous test data, the wing sections in this test were at quite different angles of attack from neighboring sections over a large portion of the run. This resulted in large 3-D flow characteristics, with (it is assumed) tip vortices being generated at the boundary between wing sections.

As seen in Fig. 15, there is a similarly large range of lift force prediction between the different models. However, in this case, none of the models accurately predicts the loads, especially in the first half of the test run. In particular, the quasi-steady models from Eqs. (4–7) all demonstrate very large delayed stall peaks at $t \approx 0.3$ s and 1.0 s where the proximal and distal angles rotate upward. However, the

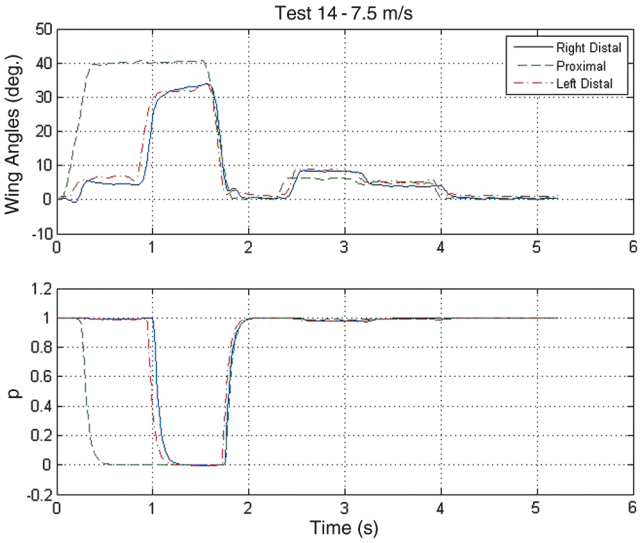

Fig. 14 Wing section angles (splined) and aerodynamic state parameter p for test 14.

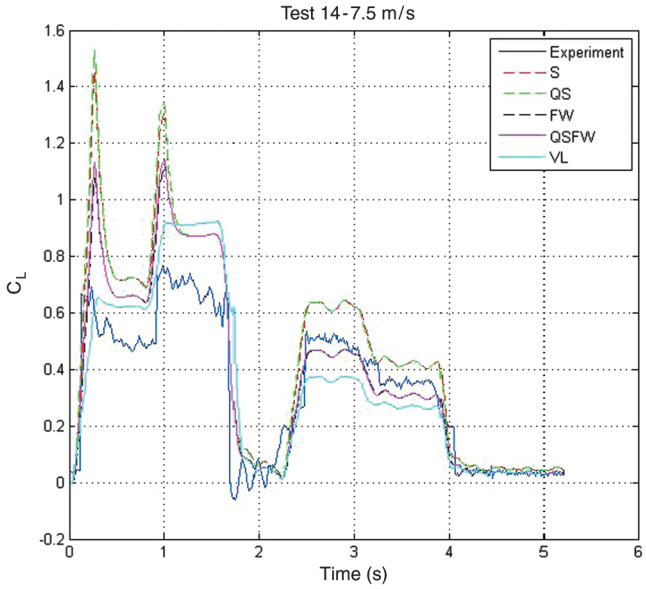

Fig. 15 Comparison of lift coefficient computations for test 14.

vortex-lattice model displays absolutely no delayed stall effect. This suggests that there may be more significant 3-D effects when there are large gaps between the wings. It is unclear whether this means that the vortices cause separation to occur earlier or whether there is some other fluid behavior that preempts the delay in separation to occur.

These efforts represent good initial steps toward the design of a perching MAV. Clearly, an actual vehicle must include many components not accounted for here, such as the introduction of secondary high lift devices or other wing degrees of freedom. Researchers at Oxford University studying bird landing behavior [1] demonstrate that covert feathers on the underside of the wing LE passively deploy much like Kruger flaps in order to increase lift at very high angles of attack. Additionally, the body of the current model was fixed in place, while future versions must include both a horizontal tail and a body capable of rotating with the wings. Since the current version is not flight capable, future versions must also allow for the volume and weight of all necessary flight systems.

VII. Conclusions

This paper addresses unsteady, transient aerodynamic models for load predictions on surfaces near and above stall. Wind-tunnel results from a simple model are presented to explore some of the key features of the aerodynamic force and moment coefficients over a range of tunnel velocities and wing rotation rates, from which specific flow behaviors can be deduced. Specifically, delayed stall effects as wings are rotated in an angle of attack beyond stall contribute significantly to the lift developed while negative pitching moments also increase significantly at the same time.

To predict these effects, an aerodynamic state time delay that combines loads from attached and separated flow regimes based on the angle-of-attack time histories is used to model this effect. The state model is agnostic with respect to predictions of the attached and separated force coefficients, meaning that anything from static 2-D lift curve slopes up to 3-D vortex-lattice methods can be used for predictions of force coefficients. The results of this demonstrate that, depending on the model complexity and geometry, 2-D models may be sufficient for transient load predictions. However, for more complex geometry incorporating separate wing sections at vastly different angles of attack and motions, 3-D methods will most likely be required.

Acknowledgments

The authors would like to thank Pamela Prater, of the University of West Florida Electrical and Computer Engineering Department, and Jud Babcock, of the U.S. Air Force Research Laboratory, Eglin Air Force Base, for their hard work and assistance with testing and postprocessing of the data.

References

[1] Carruthers, A. C., Thomas, A. L. R., and Taylor, G. K., "Automatic Aeroelastic Devices in the Wings of a Steppe Eagle Aquila Nipalensis," *Journal of Experimental Biology*, Vol. 210, 2007, pp. 4136–4149. doi:10.1242/jeb.011197

[2] Wickenheiser, A., and Garcia, E., "Longitudinal Dynamics of a Perching Aircraft," *Journal of Aircraft*, Vol. 43, No. 5, 2006, pp. 1386–1392. doi:10.2514/1.20197

[3] Wickenheiser, A., and Garcia, E., "Optimization of Perching Maneuvers Through Vehicle Morphing," *Journal of Guidance, Control, and Dynamics*, Vol. 31, No. 4, 2008, pp. 815–823. doi:10.2514/1.33819

[4] Cory, R., and Tedrake, R., "Experiments in Fixed-Wing UAV Perching," AIAA Guidance, Navigation and Control Conference and Exhibit, Honolulu, HI, AIAA Paper 2008-7256, Aug. 2008.

[5] Hoburg, W., and Tedrake, R., "System Identification of Post Stall Aerodynamics for UAV Perching," AIAA Infotech at Aerospace Conference, Seattle, WA, AIAA Paper 2009-1930, April 2009.

[6] Moore, J., and Tedrake, R., "Powerline Perching with a Fixed-Wing UAV," AIAA Infotech at Aerospace Conference, Seattle, WA, AIAA Paper 2009-1959, April 2009.

[7] Anderson, M., Perry, C. J., Hua, B. M., Olsen, D. S., Parcus, J. R., Pederson, K. M., and Jensen, D. D., "The Sticky-Pad Plane and Other Innovative Concepts for Perching UAVs," 47th AIAA Aerospace Sciences Meeting, Orlando, FL, AIAA Paper 2009-0040, Jan. 2009.

[8] Desbiens, A. L., and Cutkosky, M. R., "Landing and Perching on Vertical Surfaces with Microspines for Small Unmanned Air Vehicles," *Journal of Intelligent and Robotic Systems: Theory and Applications*, Vol. 57, Nos. 1–4, 2009, pp. 313–327. doi:10.1007/s10846-009-9377-z

[9] Garrick, I. E., "On Some Reciprocal Relations in the Theory of Non-Stationary Flows," NACA Rept. 629, 1938.

[10] McCroskey, W. J., "The Phenomenon of Dynamic Stall," NASA TM 81264, 1981.

[11] Cebeci, T., Platzer, M., Chen, H., Chang, K.-C., and Shao, J. P., *Analysis of Low-Speed Unsteady Airfoil Flows*, Horizons Publ., Long Beach, CA, 2005, pp. 31–149.

[12] Gulcat, U., "Propulsive Force of a Flexible Flapping Thin Airfoil," *Journal of Aircraft*, Vol. 46, No. 2, March–April 2009, pp. 465–473. doi:10.2514/1.35310

[13] Magill, J., Bachmann, M., Rixon, G., and McManus, K., "Dynamic Stall Control Using a Model-Based Observer," *Journal of Aircraft*, Vol. 40, No. 2, March–April 2003, pp. 355–362. doi:10.2514/2.3100

[14] Ol, M., Altman, A., Eldredge, J., Garmann, D., and Lian, Y., "Résumé of the AIAA FDTC Low Reynolds Number Discussion Group's Canonical Cases," 48th AIAA Aerospace Sciences Meeting, Orlando, FL, AIAA Paper 2010-1085, Jan. 2010.

[15] Ahuja, S., Rowley, C. W., Kevrekidis, I. G., Wei, M., Colonius, T., and Tadmor, G., "Low-Dimensional Models for Control of Leading-Edge Vortices: Equilibria and Linearized Models," 45th AIAA Aerospace Sciences Meeting, Reno, NV, AIAA Paper 2007-709, Jan. 2007.

[16] Brunton, S. L., Rowley, C. W., Taira, K., Colonius, T., Collins, J., and Williams, D. R., "Unsteady Aerodynamic Forces on Small-scale Wings: Experiments, Simulations and Models," 46th AIAA Aerospace Sciences Meeting, Reno, NV, AIAA Paper 2008-0520, Jan. 2008.

[17] Lukens, J. M., Reich, G. W., and Sanders, B., "Wing Mechanization Design and Wind Tunnel Testing for a Perching Micro Air Vehicle," *Advances in Science and Technology*, Vol. 56, June 2008, pp. 589–594. doi:10.4028/www.scientific.net/AST.56.589

[18] Lukens, J. M., Reich, G. W., and Sanders, B., "Wing Mechanization Design and Analysis for a Perching Micro Air Vehicle," 16th AIAA/ASME/AHS Adaptive Structures Conference, Schaumburg, IL, AIAA Paper 2008-1794, April 2008.

[19] Reich, G. W., Wojnar, O., and Albertani, R., "Aerodynamic Performance of a Notional Perching MAV Design," 47th AIAA Aerospace Sciences Meeting, Orlando, FL, AIAA Paper 2009-0063, Jan. 2009.

[20] Reich, G. W., Eastep, F. E., and Altman, A., "Transient Post-Stall Aerodynamic Modeling For Extreme Maneuvers in MAVs," *Proceedings of the International Forum on Aeroelasticity and Structural Dynamics*, edited by R. Kolonay, IFASD Paper 2009-141, Seattle, WA, June 2009.

[21] Tennekes, H., *The Simple Science of Flight*, MIT Press, Cambridge, MA, 1998, pp. 15–16, 129.

[22] Withers, P., "An Aerodynamic Analysis of Bird Wings as Fixed Aerofoils," *Journal of Experimental Biology*, Vol. 90, 1981, pp. 143–162.

[23] "Parallax Servo Controller - USB (#28823): Rev B," Ver. 3.3, Parallax, Inc., Rocklin, CA, 2005.

[24] Sheldahl, R., and Klimas, P., "Aerodynamic Characteristics of Seven Symmetrical Airfoil Sections Through 180-Degree Angle of Attack for Use in Aerodynamic Analysis of Vertical Axis Wind Turbines," Sandia National Labs., TR SAND 80-2114, Albuquerque, NM, 1981.

[25] Ostowari, C., and Naik, D., "Post-Stall Wind Tunnel Data for NACA 44XX Series Airfoil Sections," Solar Energy Research Institute, TR SERI/STR-217-2559, Golden, CO, 1985.

[26] Penncuick, C. J., "Wingbeat Frequency of Birds in Steady Cruising Flight: New Data and Improved Predictions," *Journal of Experimental Biology*, Vol. 199, 1996, pp. 1613–1618.

[27] Goman, M., and Khrabrov, A., "State-Space Representation of Aerodynamic Characteristics of an Aircraft at High Angles of Attack," *Journal of Aircraft*, Vol. 31, No. 5, 1994, pp. 1109–1115. doi:10.2514/3.46618

[28] Reich, G. W., Bowman, J. S., Sanders, B., and Frank, G. J., "Development of an Integrated Aeroelastic Multi-Body Morphing Simulation Tool," 14th AIAA/ASME/AHS Adaptive Structures Conference, Newport, RI, AIAA Paper 2006-1892, May 2006.